

Comparison of Edge Detection Algorithms for Automated Radiographic Measurement of the Carrying Angle

Mason AlNouri¹, Jasim Al Saei¹, Manaf Younis¹, Fadi Bouri¹, Mohamed Ali Al Habash¹,
Mohammed Hamza Shah² and Mohammed Al Dosari³

¹Hamad Medical Corporation, Department of Orthopedic Surgery, Doha, Qatar

²Hamad Medical Corporation, Department of Radiology, Doha, Qatar

³Hamad Medical Corporation, Bone and Joint Center, Doha, Qatar

mya2002@qatar-med.cornell.edu; jalsaei@hamad.qa; myounis1@hamad.qa; fbouri@hamad.qa;
malhabash@hamad.qa; mshah1@hamad.qa; maldosari1@hamad.qa

ABSTRACT

Many geometrical angles are measured directly on bone radiographs and are difficult to recall, we wanted to explore an automatic method of measurement. Edge detection was needed to determine bone edges and use them for calculation. There is no consensus on which is the best one for use in skeletal radiographs. We decided to compare commonly used edge detection methods qualitatively and quantitatively for measuring the carrying angle of the elbow using a framework we developed in PHP: Hypertext Preprocessor. Five-Hundred patients' elbow radiographs were collected. They were run through the measurement algorithm using the following edge detection methods: Sobel, Scharr, Prewitt, Frei-Chen, Kirsch, Robinson, Difference of Gaussians (DoG), Laplacian of Gaussian (LoG), Canny, Hough. Five observers manually measured the carrying angle. Results were compared using Intraclass Correlation Coefficient (ICC), Regression Analysis and Validity calculation. The Robinson algorithm was best in the qualitative analysis. Observer ICC was 0.643 which showed a strong agreement. Quantitative analysis revealed that, developing bone caused a significant bias compared to mature bone and DoG algorithm was the best due to low bias, high validity and low processing time. Automated radiographic measurement of the carrying angle of the elbow is a feasible and reliable process.

Keywords: edge detection; carrying angle; elbow; automation; radiographic

1 Introduction

Musculoskeletal imaging encompasses many geometrical angle measurements made directly on bone radiographs, these are usually measured by orthopedic surgeons or diagnostic radiologists as part of their assessment. Unfortunately, there are many angles in common use which vary in their clinical significance as well as their observational reliability [1, 2], and it is sometimes difficult and time consuming to recall and ascertain them all. For that reason, an automated approach may be useful to aid in measurements and assist clinicians in their diagnostic evaluations. In order to achieve automation, a framework has to be explored and set, along which a computer may work upon, for that purpose.

DOI: 10.14738/jbemi.26.1753

Publication Date: 28th December 2015

URL: <http://dx.doi.org/10.14738/jbemi.26.1753>

There are multiple methods available for computers that enable them to read and understand images. One notable example of such methods is edge detection, which works by identifying and isolating edges inside an image. Edges are characterized by a substantial difference in intensity across a local area. Edge detection is considered an important and primary step in many analyses and for that reason, it is under continuous research. [3] Its operators and algorithms have been extensively employed in the digital analysis of images from various kinds of medical imaging techniques such as: radiography [4-8], mammography [9], ultrasonography [10, 11], echocardiography [12], computed tomography [13], magnetic resonance [14-17], radioisotope scanning [18], positron emission tomography [19], optical coherence tomography [20, 21], near-infrared [22], fundography [23-27], angiography [28], microscopy [29], confocal microscopy [30-32] and prosthetic vision [33].

Many methods and variations exist in the processes used to achieve the detection and some were found to be more effective than others for analyzing different types of images. For instance in orthopantograms, the Canny algorithm was found to be superior to other tested common methods for qualitative landmark detection [4]. In chest radiographs the Sobel operator was found to be superior to the Roberts operator in detecting edges; however, the Canny algorithm, amongst other common methods, was not studied [34]. In retinal images, one study found the Kirsch operator to be superior to other methods, including the Canny algorithm, in blood vessel edge segmentation [23]. Whereas another study, which did not test the Kirsch operator, found the Canny algorithm to be superior among common methods but inferior to a newly proposed fusion algorithm in accurately delineating blood vessels [24]. Nevertheless, the literature lacks a large scale study that specifically tests edge detection techniques, both quantitatively and qualitatively, for use in analyzing medical images. Additionally, the vast majority of studies carried out on edge detection employed high-level mathematical packages, such as the MATLAB environment [4, 5, 7, 10, 15, 19, 25-27, 30], to perform their analyses; however, although these programs are powerful, they are not readily available for wide use and are not always needed for simpler functions.

In order to address the aforementioned issues, we decided to compare edge detection methods after incorporating them into an algorithm that automatically measures the carrying angle of the elbow, which is defined as the angle made between the axis of the upper arm and that of the forearm [35]. This angle was chosen mainly because of the high precision obtained through radiographic versus goniometric measurements [36] in addition to its good inter-observer reliability [37]. Furthermore, the algorithm was coded in PHP: Hypertext Preprocessor (PHP), a widely used web scripting language, to allow for ease of access and simpler usage.

The aim of this study was to:

1. Compare the reliability of various edge detection operators and algorithms qualitatively and quantitatively in the context of automatic measurements of the carrying angle
2. Check for some patient-specific variables that may affect the reliability of edge detection at the elbow.
3. Develop a framework by which automated measuring of the carrying angle could be made through an easy digital environment

2 Methods

2.1 Image Collection

Five-hundred digitized elbow radiographic images were obtained by searching the hospital’s PACS v3.7.3.9 (Picture Archiving and Communication System) database for all stored elbow studies. Since the images were obtained retrospectively with no risk to patients, no ethical approval was required to carry out the study and informed consent was waived after the study was reviewed by the local research committee at the Medical Research Center in accordance with the hospital’s rules and regulations policy for research in section III titled “Consent Procedure”, subsection 8.3 titled “Types of Consent”. Furthermore, approval to access the stored images was given by the same committee after completing their review.

The search results were then sorted by age and manually selected in order to meet the required quota of one-hundred images, divided into fifty males and fifty females, of patients’ elbows taken at each of the following ages: one, five, nine, eleven and twenty to forty. These ages were selected to approximately represent the different stages of ossification [38]. *Table 1* shows the patient distribution.

Table 1 Overall distribution of patient and variables for elbow radiographs

| Age | Number of Patient Radiographs | | | |
|---------------------------------------|-------------------------------|---------|------|-------|
| | Sex | | Side | |
| | Males | Females | Left | Right |
| 1 | 50 | 50 | 42 | 58 |
| 5 | 50 | 50 | 55 | 45 |
| 9 | 50 | 50 | 57 | 43 |
| 11 | 50 | 50 | 51 | 49 |
| 20-40 | 50 | 50 | 49 | 51 |
| Totals | 250 | 250 | 254 | 246 |
| Total Patient Radiographs: 500 | | | | |

After a patient’s radiograph was selected, it was viewed on a monitor set at a screen resolution of 1024 × 768 using the PACS Viewer Component v3.7.3.9078. Any image containing the following criteria was excluded:-

- Major deformities of the humerus, radius or ulna
- Displaced fractures
- Bone lesions
- Anterior-posterior view taken in forearm pronation or any other inappropriate position
- Visible bone implants
- External interference such as slabs, casts or an examiner’s hand

The brightness and contrast settings of the radiograph were altered within the viewer in order to minimize soft-tissue and skin interference and maximize visibility of the bone. Subsequently, the screen was captured using the ‘Print Screen’ function, pasted into Microsoft Windows Paint v6.1 and further cropping of the corners was carried out. Finally, all remaining labels were removed from the image and a

scale was applied in order to approximately obtain a width of 400 and a height of 500. The end result, as shown in *Figure 1*, was then stored as a png image in a folder and recorded in a spreadsheet with a study specific identifier along with the patient's age, sex and the limb side.



Figure 1 A sample Anterior-Posterior elbow radiograph to be used as an input image for automated measurement

2.2 Measurement Algorithm

The algorithm used to measure the carrying angle from the input images was programmed in PHP and run on the PHP Engine v5.5.8 using an Intel i7 Core 3.46GHz 8.0GB RAM 64-bit Windows 7 Professional system in order to centralize the processing of images on a single server while allowing various users to utilize the service.

Steps involved in the algorithm:-

- Step-1 Create an array of all images in the specified system folder
- Step-2 Enter a loop that stops after all the images have been processed
- Step-3 Apply the edge detection algorithm to the image
- Step-4 Loop through all the image's pixels and eliminate pixels according to a set threshold
- Step-5 Create different groups for all remaining pixels adjacent to each other
- Step-6 Collect the first six groups which span the highest value for vertical range
- Step-7 Define the bone borders based on each group's location within the image space
- Step-8 Estimate the central axis of the humerus and ulna based on the defined borders
- Step-9 Calculate the carrying angle of the elbow based on the bone axes and store the result
- Step-10 Go to Step 2 or end the loop and output all results

All five-hundred images were placed in a folder and run through the algorithm a total of eight times to test all the edge detection methods included in this study.

2.3 Edge Detection Algorithms

All the following algorithms were chosen due to their common use and were tested in this study by being incorporated into the measurement algorithm in 2.2 at Step 3. The threshold values in 2.2 at Step 4 were different for each algorithm and they were determined by testing the algorithm on ten random elbow radiographs and selecting the output with the most accurate values obtained for the carrying angle.

2.3.1 Sobel Operator

The Sobel Operator was applied by carrying out a two dimensional image convolution in both the vertical and the horizontal direction. The following matrices were used:-

$$F_x = \begin{vmatrix} -1 & 0 & +1 \\ -2 & 0 & +2 \\ -1 & 0 & +1 \end{vmatrix} \quad F_y = \begin{vmatrix} +1 & +2 & +1 \\ 0 & 0 & 0 \\ -1 & -2 & -1 \end{vmatrix} \quad (1)$$

F_x is the horizontal derivative and F_y is the vertical derivative at a specific point in the image

2.3.2 Scharr Operator

The Scharr Operator was applied in similar way to the Sobel in 2.3.1 using the following matrices:-

$$F_x = \begin{vmatrix} -3 & 0 & +3 \\ -10 & 0 & +10 \\ -3 & 0 & +3 \end{vmatrix} \quad F_y = \begin{vmatrix} +3 & +10 & +3 \\ 0 & 0 & 0 \\ -3 & -10 & -3 \end{vmatrix} \quad (2)$$

2.3.3 Prewitt Operator

The Prewitt Operator was applied in similar way to the Sobel in 2.3.1 using the following matrices:-

$$F_x = \begin{vmatrix} -1 & 0 & +1 \\ -1 & 0 & +1 \\ -1 & 0 & +1 \end{vmatrix} \quad F_y = \begin{vmatrix} +1 & +1 & +1 \\ 0 & 0 & 0 \\ -1 & -1 & -1 \end{vmatrix} \quad (3)$$

2.3.4 Frei-Chen Filter

The Frei-Chen Filter was applied by performing nine separate image convolutions using the nine matrices below:-

$$\begin{aligned} W_1 &= \frac{1}{2\sqrt{2}} \begin{vmatrix} +1 & +\sqrt{2} & +1 \\ 0 & 0 & 0 \\ -1 & -\sqrt{2} & -1 \end{vmatrix} & W_2 &= \frac{1}{2\sqrt{2}} \begin{vmatrix} +1 & 0 & -1 \\ +\sqrt{2} & 0 & -\sqrt{2} \\ +1 & 0 & -1 \end{vmatrix} & W_3 &= \frac{1}{2\sqrt{2}} \begin{vmatrix} 0 & -1 & +\sqrt{2} \\ +1 & 0 & -1 \\ -\sqrt{2} & +1 & 0 \end{vmatrix} \\ W_4 &= \frac{1}{2\sqrt{2}} \begin{vmatrix} +\sqrt{2} & -1 & 0 \\ -1 & 0 & +1 \\ 0 & +1 & -\sqrt{2} \end{vmatrix} & W_5 &= \frac{1}{2} \begin{vmatrix} 0 & +1 & 0 \\ -1 & 0 & -1 \\ 0 & +1 & 0 \end{vmatrix} & W_6 &= \frac{1}{2} \begin{vmatrix} -1 & 0 & +1 \\ 0 & 0 & 0 \\ +1 & 0 & -1 \end{vmatrix} \\ W_7 &= \frac{1}{6} \begin{vmatrix} +1 & -2 & +1 \\ -2 & +4 & -2 \\ +1 & -2 & +1 \end{vmatrix} & W_8 &= \frac{1}{6} \begin{vmatrix} -2 & +1 & -2 \\ +1 & +4 & +1 \\ -2 & +1 & -2 \end{vmatrix} & W_9 &= \frac{1}{3} \begin{vmatrix} +1 & +1 & +1 \\ +1 & +1 & +1 \\ +1 & +1 & +1 \end{vmatrix} \end{aligned} \quad (4)$$

This was then followed by the calculation of the weighted average from the results of the image convolutions.

2.3.5 Kirsch Operator

The Kirsch Operator was applied by rotating a single kernel matrix through eight different compass directions and calculating the final sum resulting from the addition of all the image convolutions in all directions. The kernel matrix is given below:-

$$K_1 = \begin{bmatrix} +5 & +5 & +5 \\ -3 & 0 & -3 \\ -3 & -3 & -3 \end{bmatrix} \quad (5)$$

2.3.6 Robinson Operator

The Robinson Operator was applied in similar way to the Kirsch Operator in 2.3.5 using the following kernel matrix:-

$$R_1 = \begin{bmatrix} +1 & +1 & +1 \\ +1 & -2 & +1 \\ -1 & -1 & -1 \end{bmatrix} \quad (6)$$

2.3.7 Difference of Gaussians

The Difference of Gaussians (DoG) was applied by using two Gaussian blur masks at different intensities, followed by subtracting their results. The Gaussian function and the matrix used for convolution is given below:-

$$G(x, y) = \frac{1}{\sqrt{2\pi\sigma^2}} e^{-\frac{x^2+y^2}{2\sigma^2}} \quad G = \begin{bmatrix} +1 & +2 & +1 \\ +2 & +4 & +2 \\ +1 & +2 & +1 \end{bmatrix} \quad (7)$$

Where x is the horizontal and y is the vertical coordinate inside an image. σ is the standard deviation of the Gaussian function.

2.3.8 Laplacian of Gaussian

The Laplacian of Gaussian (LoG) was applied by using a Gaussian blur mask on the image along with a Laplacian kernel. The Gaussian, Laplacian and combined functions as well as the matrix used for convolution are given below:-

$$G(x, y) = \frac{1}{\sqrt{2\pi\sigma^2}} e^{-\frac{x^2+y^2}{2\sigma^2}} \quad (8)$$

$$L(x, y) = \frac{1}{\sqrt{2\pi\sigma^2}} e^{-\frac{x^2+y^2}{2\sigma^2}} \quad (9)$$

$$LoG(x, y) = -\frac{1}{\pi\sigma^4} \left[1 - \frac{x^2 + y^2}{2\sigma^2} \right] e^{-\frac{x^2 + y^2}{2\sigma^2}}$$

$$LoG = \begin{bmatrix} 0 & 0 & -1 & 0 & 0 \\ 0 & -1 & -2 & -1 & 0 \\ -1 & -2 & +16 & -2 & -1 \\ 0 & -1 & -2 & -1 & 0 \\ 0 & 0 & -1 & 0 & 0 \end{bmatrix}$$

2.3.9 Canny Algorithm

The Canny Algorithm was applied by following the four steps:-

1. Blur the image using the following Gaussian mask

$$G = \begin{bmatrix} +2 & +4 & +5 & +4 & +2 \\ +4 & +9 & +12 & +9 & +4 \\ +5 & +12 & +15 & +12 & +5 \\ +4 & +9 & +12 & +9 & +4 \\ +2 & +4 & +5 & +4 & +2 \end{bmatrix} \quad (10)$$

2. Apply the Sobel Operator as in 2.3.1 then calculate the gradient angle using the equation

$$\theta = \text{atan2}(y, x)$$

Where θ is the gradient angle, y is the vertical gradient and x is the horizontal gradient

3. Suppress non-maximum pixels within the image based on the neighboring pixels
4. Apply a double threshold to the remaining pixels

2.3.10 Hough Transform

The Hough Transform was applied through the following steps:-

1. Apply the Canny edge detector as in 2.3.9
2. Create the Hough space for remaining pixels using the following equation

$$r = x\cos(\theta) + y\sin(\theta) \quad (11)$$

Where r is the distance of the line from the origin, θ is the slope of that line and x, y are the coordinates of an arbitrary point on that line

3. Collect votes from the image's pixels for all the lines in the Hough space
4. Dehough the lines with the most votes by using their predetermined line equation

2.4 Observer Measurements

Five different observers were each given the 500 images obtained from the collection in 2.1 in order to manually measure the carrying angle using the radiographic method. The observers were 'blinded' by not being given any details about the automatic measurement algorithm until after the completion of all manual measurements. The angle was determined by drawing the long axis of the humerus and the long axis of the ulna followed by measuring the angle made by their bisection as shown in *Figure 2* [37]. Afterwards, the measurements were recorded in a MySQL database for later comparison to the values obtained from the algorithm.



Figure 2 Radiograph showing the labelled long axes of the Humerus and Ulna with the formed Carrying Angle

2.5 Algorithm Validity

The validity of all automated measurements was calculated by comparing all of the readings to the real value of the carrying angle, which was assumed to be the mean of all observer measurements, in order to check if they fall within a $\pm 5^\circ$ range in which case the readings would be considered correct. This range was chosen based on the approximate error observed in different readings of the carrying angle [36, 49]. A percent validity was then obtained through dividing the total number of correct readings by the total number of readings and then multiplying by 100.

2.6 Statistical Analysis

All data were analyzed within the SPSS program (v20, SPSS Inc., Chicago, IL, USA). All p values ≤ 0.05 were considered statistically significant. In order to evaluate the consistency of observer measurements, the Intraclass Correlation Coefficient (ICC) was calculated for single readings. Based on the values of the ICC the following agreement ratings were selected: poor (0-0.200), fair (0.201-0.400), moderate (0.401-0.600), strong (0.601-0.800) and excellent (>0.801) [50]. The 95% confidence interval range was also quantified. Subsequently, the manual and automated readings obtained for the carrying angle were compared for any biases using linear regression analyses. This was carried out by first calculating the mean of all observer readings for a single elbow, the result was considered the real value of the carrying angle. After that, the difference as well as the average of the real value and the algorithm's

measurement was calculated. The average was set to be the independent variable and the difference was set to be the dependent variable. Consequently, the measurements were then split by variables of age, sex and side and the regression analysis was carried out for each one.

3 Results

3.1 Qualitative Comparison

All the output images were checked in order to identify which edge detection method included the most accurately defined bone edge with the least noise. Samples can be seen in *Figure 3*. With regards to the output from the Sobel, Scharr and Prewitt Operators, the level of noise and edge accuracy was almost similar with only a negligible reduction in noise by the Scharr Operator. When compared to the prior three, the Frei-Chen output showed a largely reduced external noise but a greatly increased internal bone noise; moreover, the edges were generally less accurate and much thicker than all other outputs. The Kirsch and Robinson Operators were superior to all other methods in both the noise level and the edge accuracy. Compared to each other, the Robinson output exhibited slightly less noise than the Kirsch output but no significant change was noted in edge thickness or accuracy. The DoG output was largely similar to the Frei-Chen output with a notable increase in noise as well as edge thickness. The LoG output was similar to the three initially mentioned operators in terms of edge accuracy, the thickness was slightly increased; however, there was a small decrease in external noise coupled with a large increase in internal noise. The Canny output revealed a highly accurate thin edge but the image contained more noise, both internal and external, than the Kirsch and Robinson output images. Finally, the Hough output revealed a thick edge which was less accurate than all other outputs, with little internal and external noise.

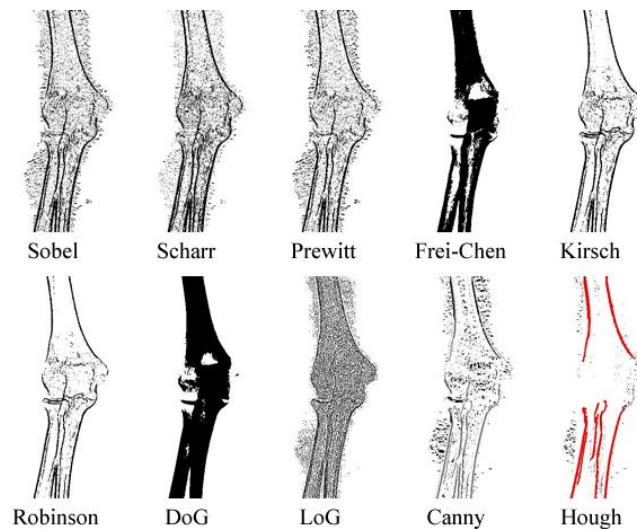


Figure 3 Sample output images from all ten edge detection methods obtained from the input image in *Figure 1*

In summary, the Robinson Operator was superior to other methods for edge accuracy and noise level. *Table 2* shows the relative rankings of all edge detection methods.

Table 2 Relative rankings of all ten edge detection methods with regards to various aspects of qualitative analysis. Ascending order (A) Descending order (D)

| Edge Accuracy (D) | Edge Thickness (A) | Internal Noise (A) | External Noise (A) |
|-------------------|--------------------|--------------------|--------------------|
| Robinson | Canny | Robinson | Robinson |
| Kirsch | Robinson | Kirsch | Kirsch |
| Canny | Kirsch | Hough | DoG |
| LoG | Prewitt | Canny | Frei-Chen |
| Scharr | Sobel | Prewitt | Hough |
| Sobel | Scharr | Sobel | Canny |
| Prewitt | LoG | Scharr | LoG |
| DoG | Hough | LoG | Scharr |
| Frei-Chen | Frei-Chen | Frei-Chen | Prewitt |
| Hough | DoG | DoG | Sobel |

3.2 Observer Comparison

The ICC for all observer measurements was found to be 0.643 (95% CI: 0.547 to 0.718). This indicated a strong agreement based on the predefined ratings. The ICC values were also calculated after separating the observer readings by variables of age, sex and side and, although there were some differences in the ICC values, they did not show any statistical significance based on the confidence interval ranges. ICC values are shown in *Table 3*.

Table 3 The Intraclass Correlation Coefficients (ICC) and 95% Confidence Intervals calculated based on observer carrying angle measurements for all radiographs which was divided by variables age, sex and side

| Group | ICC | 95% Confidence Interval | |
|------------|-------|-------------------------|-------|
| | | Lower | Upper |
| Age 1 | 0.546 | 0.410 | 0.663 |
| Age 5 | 0.589 | 0.456 | 0.699 |
| Age 9 | 0.607 | 0.437 | 0.731 |
| Age 11 | 0.738 | 0.641 | 0.813 |
| Age 20-40 | 0.755 | 0.632 | 0.837 |
| Males | 0.598 | 0.486 | 0.687 |
| Females | 0.691 | 0.599 | 0.762 |
| Left Side | 0.651 | 0.542 | 0.734 |
| Right Side | 0.635 | 0.527 | 0.719 |
| Overall | 0.643 | 0.547 | 0.718 |

3.3 Algorithm Comparisons

The measurements for each edge detection method, as well as their final mean, were checked for bias, validity and processing time.

3.3.1 Sobel Operator Results

The Sobel measurements obtained an overall B value of -0.729 (95% CI: -0.815 to -0.643 $p < 0.001$) with an overall 67% validity and an average 3min 27s of processing time per image. Further analysis based on variables revealed no statistically significant differences in any reading. *Table 4* shows the detailed results obtained from each variable.

Table 4 Results for the Sobel Operator measurements showing B values, Standard Error, 95% Confidence Intervals, p values and validity, all divided by the variables age, sex and side

| Group | B | Standard Error | 95% Confidence Interval | | p value | Validity |
|------------|--------|----------------|-------------------------|--------|---------|----------|
| | | | Lower | Upper | | |
| Age 1 | -0.794 | 0.101 | -0.994 | -0.594 | <0.001 | 69% |
| Age 5 | -0.791 | 0.095 | -0.980 | -0.602 | <0.001 | 61% |
| Age 9 | -0.735 | 0.087 | -0.908 | -0.562 | <0.001 | 66% |
| Age 11 | -0.548 | 0.099 | -0.745 | -0.351 | <0.001 | 69% |
| Age 20-40 | -0.841 | 0.121 | -01.08 | -0.601 | <0.001 | 69% |
| Males | -0.759 | 0.067 | -0.890 | -0.628 | <0.001 | 66% |
| Females | -0.703 | 0.058 | -0.818 | -0.588 | <0.001 | 67% |
| Left Side | -0.658 | 0.057 | -0.771 | -0.545 | <0.001 | 66% |
| Right Side | -0.816 | 0.067 | -0.949 | -0.684 | <0.001 | 68% |
| Overall | -0.729 | 0.044 | -0.815 | -0.643 | <0.001 | 67% |

3.3.2 Scharr Operator Results

The Scharr measurements obtained an overall B value of -0.633 (95% CI: -0.717 to -0.548 $p<0.001$) with an overall 72% validity and an average 3min 38s of processing time per image. Further analysis based on variables revealed a higher validity result in the Age 20-40 group at 88%. *Table 5* shows the detailed results obtained from each variable.

Table 5 Results for the Scharr Operator measurements showing B values, Standard Error, 95% Confidence Intervals, p values and validity all divided by the variables age, sex and side

| Group | B | Standard Error | 95% Confidence Interval | | p value | Validity |
|------------|--------|----------------|-------------------------|--------|---------|----------|
| | | | Lower | Upper | | |
| Age 1 | -0.709 | 0.093 | -0.894 | -0.525 | <0.001 | 73% |
| Age 5 | -0.785 | 0.100 | -0.983 | -0.587 | <0.001 | 61% |
| Age 9 | -0.664 | 0.110 | -0.883 | -0.444 | <0.001 | 61% |
| Age 11 | -0.472 | 0.093 | -0.656 | -0.288 | <0.001 | 75% |
| Age 20-40 | -0.537 | 0.083 | -0.702 | -0.373 | <0.001 | 88% |
| Males | -0.603 | 0.064 | -0.729 | -0.477 | <0.001 | 72% |
| Females | -0.646 | 0.059 | -0.762 | -0.531 | <0.001 | 72% |
| Left Side | -0.552 | 0.056 | -0.663 | -0.441 | <0.001 | 73% |
| Right Side | -0.729 | 0.066 | -0.858 | -0.600 | <0.001 | 70% |
| Overall | -0.633 | 0.043 | -0.717 | -0.548 | <0.001 | 72% |

3.3.3 Prewitt Operator Results

The Prewitt measurements obtained an overall B value of -0.730 (95% CI: -0.819 to -0.642 $p<0.001$) with an overall 65% validity and an average 3min 19s of processing time per image. Further analysis based on variables revealed a significantly lower B value when comparing the Age 1 group (B = -0.956 95% CI: -1.157 to -0.755 $p<0.001$) and the Left Side group (B = -0.631 95% CI: -0.749 to -0.512 $p<0.001$). *Table 6* shows the detailed results obtained from each variable.

Table 6 Results for the Prewitt Operator measurements showing B values, Standard Error, 95% Confidence Intervals, p values and validity all divided by the variables age, sex and side

| Group | B | Standard Error | 95% Confidence Interval | | p value | Validity |
|------------|--------|----------------|-------------------------|--------|---------|----------|
| | | | Lower | Upper | | |
| Age 1 | -0.956 | 0.101 | -1.157 | -0.755 | <0.001 | 69% |
| Age 5 | -0.602 | 0.080 | -0.761 | -0.444 | <0.001 | 65% |
| Age 9 | -0.641 | 0.099 | -0.838 | -0.445 | <0.001 | 64% |
| Age 11 | -0.596 | 0.100 | -0.795 | -0.397 | <0.001 | 63% |
| Age 20-40 | -0.927 | 0.127 | -1.179 | -0.674 | <0.001 | 64% |
| Males | -0.722 | 0.061 | -0.843 | -0.602 | <0.001 | 66% |
| Females | -0.739 | 0.066 | -0.869 | -0.609 | <0.001 | 64% |
| Left Side | -0.631 | 0.060 | -0.749 | -0.512 | <0.001 | 67% |
| Right Side | -0.846 | 0.067 | -0.978 | -0.714 | <0.001 | 63% |
| Overall | -0.730 | 0.045 | -0.819 | -0.642 | <0.001 | 65% |

3.3.4 Frei-Chen Filter Results

The Frei-Chen measurements obtained an overall B value of -0.539 (95% CI: -0.615 to -0.462 $p<0.001$) with an overall 75% validity and an average 1min 16s of processing time per image. Further analysis based on variables revealed a significantly higher B value in both the Age 11 group (B = -0.251 95% CI: -0.393 to -0.109 $p=0.001$) and the Age 20-40 group (B = -0.327 95% CI: -0.438 to -0.215 $p<0.001$) with a significantly lower B value in the Age 1 group (B = -0.879 95% CI: -1.071 to -0.687 $p<0.001$). Similarly, the validity results were much higher in the Age 11 (83%) and Age 20-40 group (95%) compared to the Age 1 group (61%). Table 7 shows the detailed results obtained from each variable.

Table 7 Results for the Frei-Chen Filter measurements showing B values, Standard Error, 95% Confidence Intervals, p values and validity all divided by the variables age, sex and side

| Group | B | Standard Error | 95% Confidence Interval | | p value | Validity |
|------------|--------|----------------|-------------------------|--------|---------|----------|
| | | | Lower | Upper | | |
| Age 1 | -0.879 | 0.097 | -1.071 | -0.687 | <0.001 | 61% |
| Age 5 | -0.671 | 0.094 | -0.858 | -0.483 | <0.001 | 69% |
| Age 9 | -0.512 | 0.084 | -0.679 | -0.345 | <0.001 | 69% |
| Age 11 | -0.251 | 0.072 | -0.393 | -0.109 | 0.001 | 83% |
| Age 20-40 | -0.327 | 0.056 | -0.438 | -0.215 | <0.001 | 95% |
| Males | -0.543 | 0.056 | -0.653 | -0.432 | <0.001 | 72% |
| Females | -0.535 | 0.055 | -0.642 | -0.427 | <0.001 | 78% |
| Left Side | -0.404 | 0.048 | -0.500 | -0.309 | <0.001 | 79% |
| Right Side | -0.682 | 0.061 | -0.801 | -0.562 | <0.001 | 72% |
| Overall | -0.539 | 0.039 | -0.615 | -0.462 | <0.001 | 75% |

3.3.5 Kirsch Operator Results

The Kirsch measurements obtained an overall B value of -0.432 (95% CI: -0.505 to -0.358 $p<0.001$) with an overall 77% validity and an average 1min 20s of processing time per image. Further analysis based on variables revealed a significantly lower B value when comparing the Age 1 group (B = -0.621 95% CI: -

0.791 to -0.451 $p < 0.001$) and the Age 11 group (B = -0.298 95% CI: -0.438 to -0.159 $p < 0.001$). Moreover, the validity was higher in the Age 20-40 group (85%) compared to the Age 9 group (67%). *Table 8* shows the detailed results obtained from each variable.

Table 8 Results for the Kirsch Operator measurements showing B values, Standard Error, 95% Confidence Intervals, p values and validity all divided by the variables age, sex and side

| Group | B | Standard Error | 95% Confidence Interval | | p value | Validity |
|------------|--------|----------------|-------------------------|--------|---------|----------|
| | | | Lower | Upper | | |
| Age 1 | -0.621 | 0.086 | -0.791 | -0.451 | <0.001 | 79% |
| Age 5 | -0.404 | 0.073 | -0.548 | -0.260 | <0.001 | 73% |
| Age 9 | -0.516 | 0.104 | -0.723 | -0.310 | <0.001 | 67% |
| Age 11 | -0.298 | 0.070 | -0.438 | -0.159 | <0.001 | 82% |
| Age 20-40 | -0.303 | 0.079 | -0.460 | -0.147 | <0.001 | 85% |
| Males | -0.455 | 0.053 | -0.559 | -0.351 | <0.001 | 77% |
| Females | -0.408 | 0.053 | -0.513 | -0.303 | <0.001 | 77% |
| Left Side | -0.405 | 0.052 | -0.506 | -0.303 | <0.001 | 76% |
| Right Side | -0.465 | 0.055 | -0.573 | -0.358 | <0.001 | 79% |
| Overall | -0.432 | 0.037 | -0.505 | -0.358 | <0.001 | 77% |

3.3.6 Robinson Operator Results

The Robinson measurements obtained an overall B value of -0.511 (95% CI: -0.597 to -0.425 $p < 0.001$) with an overall 77% validity and an average 1min 13s of processing time per image. Further analysis based on variables revealed a significantly higher B value in both the Age 11 group (B = -0.284 95% CI: -0.434 to -0.134 $p < 0.001$) and the Age 20-40 group (B = -0.389 95% CI: -0.549 to -0.230 $p < 0.001$) with a significantly lower B value in the Age 1 group (B = -0.928 95% CI: -1.181 to -0.675 $p < 0.001$). Additionally, the validity was higher in the Age 20-40 group (86%). *Table 9* shows the detailed results obtained from each variable.

Table 9 Results for the Robinson Operator measurements showing B values, Standard Error, 95% Confidence Intervals, p values and validity all divided by the variables age, sex and side

| Group | B | Standard Error | 95% Confidence Interval | | p value | Validity |
|------------|--------|----------------|-------------------------|--------|---------|----------|
| | | | Lower | Upper | | |
| Age 1 | -0.928 | 0.128 | -1.181 | -0.675 | <0.001 | 75% |
| Age 5 | -0.516 | 0.088 | -0.690 | -0.342 | <0.001 | 71% |
| Age 9 | -0.457 | 0.094 | -0.645 | -0.270 | <0.001 | 70% |
| Age 11 | -0.284 | 0.076 | -0.434 | -0.134 | <0.001 | 81% |
| Age 20-40 | -0.389 | 0.080 | -0.549 | -0.230 | <0.001 | 86% |
| Males | -0.585 | 0.061 | -0.706 | -0.464 | <0.001 | 74% |
| Females | -0.429 | 0.063 | -0.553 | -0.306 | <0.001 | 79% |
| Left Side | -0.446 | 0.059 | -0.561 | -0.330 | <0.001 | 75% |
| Right Side | -0.588 | 0.066 | -0.718 | -0.458 | <0.001 | 78% |
| Overall | -0.511 | 0.044 | -0.597 | -0.425 | <0.001 | 77% |

3.3.7 Difference of Gaussians Results

The DoG measurements obtained an overall B value of -0.487 (95% CI: -0.559 to -0.415 $p < 0.001$) with an overall 80% validity and an average 1min 33s of processing time per image. Further analysis based on variables revealed a significantly higher B value in both the Age 11 group (B = -0.226 95% CI: -0.359 to -0.093 $p = 0.001$) and the Age 20-40 group (B = -0.302 95% CI: -0.468 to -0.136 $p < 0.001$) with a significantly lower B value in the Age 1 group (B = -0.630 95% CI: -0.808 to -0.452 $p < 0.001$) and the Age 5 group (B = -0.654 95% CI: -0.810 to -0.499 $p < 0.001$). Additionally, the validity was higher in the Age 20-40 group (94%). *Table 10* shows the detailed results obtained from each variable.

Table 10 Results for the Difference of Gaussians measurements showing B values, Standard Error, 95% Confidence Intervals, p values and validity all divided by the variables age, sex and side

| Group | B | Standard Error | 95% Confidence Interval | | p value | Validity |
|------------|--------|----------------|-------------------------|--------|---------|----------|
| | | | Lower | Upper | | |
| Age 1 | -0.630 | 0.090 | -0.808 | -0.452 | <0.001 | 76% |
| Age 5 | -0.654 | 0.078 | -0.810 | -0.499 | <0.001 | 70% |
| Age 9 | -0.552 | 0.084 | -0.718 | -0.386 | <0.001 | 72% |
| Age 11 | -0.226 | 0.067 | -0.359 | -0.093 | 0.001 | 86% |
| Age 20-40 | -0.302 | 0.084 | -0.468 | -0.136 | <0.001 | 94% |
| Males | -0.538 | 0.053 | -0.643 | -0.433 | <0.001 | 76% |
| Females | -0.429 | 0.051 | -0.529 | -0.329 | <0.001 | 83% |
| Left Side | -0.434 | 0.049 | -0.529 | -0.338 | <0.001 | 80% |
| Right Side | -0.552 | 0.056 | -0.662 | -0.443 | <0.001 | 79% |
| Overall | -0.487 | 0.037 | -0.559 | -0.415 | <0.001 | 80% |

3.3.8 Laplacian of Gaussian Results

The LoG measurements obtained an overall B value of -1.024 (95% CI: -1.122 to -0.927 $p < 0.001$) with an overall 55% validity and an average 1min 37s of processing time per image. Further analysis based on variables revealed a significantly higher B value in both the Age 11 group (B = -0.495 95% CI: -0.701 to -0.290 $p < 0.001$) and the Age 9 group (B = -0.799 95% CI: -0.986 to -0.611 $p < 0.001$) with a significantly lower B value in the Age 1 group (B = -1.419 95% CI: -1.614 to -1.224 $p < 0.001$). Moreover, the validity was higher in the Age 11 group (72%) and lower in the Age 1 group (30%). *Table 11* shows the detailed results obtained from each variable.

Table 11 Results for the Laplacian of Gaussian measurements showing B values, Standard Error, 95% Confidence Intervals, p values and validity all divided by the variables age, sex and side

| Group | B | Standard Error | 95% Confidence Interval | | p value | Validity |
|------------|--------|----------------|-------------------------|--------|---------|----------|
| | | | Lower | Upper | | |
| Age 1 | -1.419 | 0.098 | -1.614 | -1.224 | <0.001 | 30% |
| Age 5 | -1.091 | 0.112 | -1.314 | -0.869 | <0.001 | 48% |
| Age 9 | -0.799 | 0.094 | -0.986 | -0.611 | <0.001 | 58% |
| Age 11 | -0.495 | 0.103 | -0.701 | -0.290 | <0.001 | 72% |
| Age 20-40 | -0.977 | 0.111 | -1.198 | -0.756 | <0.001 | 68% |
| Males | -1.089 | 0.072 | -1.231 | -0.946 | <0.001 | 50% |
| Females | -0.963 | 0.068 | -1.097 | -0.828 | <0.001 | 60% |
| Left Side | -0.943 | 0.069 | -1.079 | -0.806 | <0.001 | 54% |
| Right Side | -1.114 | 0.071 | -1.254 | -0.975 | <0.001 | 57% |
| Overall | -1.024 | 0.050 | -1.122 | -0.927 | <0.001 | 55% |

3.3.9 Canny Algorithm Results

The Canny measurements obtained an overall B value of -0.881 (95% CI: -0.978 to -0.785 $p<0.001$) with an overall 67% validity and an average 5min 3s of processing time per image. Further analysis based on variables revealed a significantly lower B value when comparing the Age 1 group (B = -1.259 95% CI: -1.494 to -1.024 $p<0.001$) and the Age 11 group (B = -0.663 95% CI: -0.883 to -0.444 $p<0.001$). Additionally, the validity was higher in the Age 20-40 group (81%). Table 12 shows the detailed results obtained from each variable.

Table 12 Results for the Canny measurements showing B values, Standard Error, 95% Confidence Intervals, p values and validity all divided by the variables age, sex and side

| Group | B | Standard Error | 95% Confidence Interval | | p value | Validity |
|------------|--------|----------------|-------------------------|--------|---------|----------|
| | | | Lower | Upper | | |
| Age 1 | -1.259 | 0.118 | -1.494 | -1.024 | <0.001 | 58% |
| Age 5 | -0.869 | 0.087 | -1.042 | -0.696 | <0.001 | 62% |
| Age 9 | -0.788 | 0.111 | -1.008 | -0.569 | <0.001 | 64% |
| Age 11 | -0.663 | 0.111 | -0.883 | -0.444 | <0.001 | 69% |
| Age 20-40 | -0.778 | 0.114 | -1.004 | -0.553 | <0.001 | 81% |
| Males | -0.895 | 0.066 | -1.026 | -0.764 | <0.001 | 65% |
| Females | -0.868 | 0.073 | -1.012 | -0.724 | <0.001 | 68% |
| Left Side | -0.889 | 0.064 | -1.016 | -0.763 | <0.001 | 63% |
| Right Side | -0.858 | 0.078 | -1.011 | -0.704 | <0.001 | 70% |
| Overall | -0.881 | 0.049 | -0.978 | -0.785 | <0.001 | 67% |

3.3.10 Hough Transform Results

The Hough measurements obtained an overall B value of -0.558 (95% CI: -0.637 to -0.479 $p<0.001$) with an overall 78% validity and an average 8min 13s of processing time per image. Further analysis based on variables revealed a significantly higher B value in the Age 11 group (B = -0.239 95% CI: -0.372 to -0.106 $p=0.001$) with a significantly lower B value in the Age 1 group (B = -1.054 95% CI: -1.249 to -0.858

$p < 0.001$). Additionally, the validity was higher in the Age 20-40 group (93%) and lower in the Age 1 group (65%). Table 13 shows the detailed results obtained from each variable.

Table 13 Results for the Hough measurements showing B values, Standard Error, 95% Confidence Intervals, p values and validity all divided by the variables age, sex and side

| Group | B | Standard Error | 95% Confidence Interval | | p value | Validity |
|------------|--------|----------------|-------------------------|--------|---------|----------|
| | | | Lower | Upper | | |
| Age 1 | -1.054 | 0.099 | -1.249 | -0.858 | <0.001 | 65% |
| Age 5 | -0.515 | 0.078 | -0.670 | -0.360 | <0.001 | 73% |
| Age 9 | -0.412 | 0.084 | -0.578 | -0.246 | <0.001 | 74% |
| Age 11 | -0.239 | 0.067 | -0.372 | -0.106 | 0.001 | 84% |
| Age 20-40 | -0.315 | 0.067 | -0.448 | -0.182 | <0.001 | 93% |
| Males | -0.586 | 0.054 | -0.692 | -0.479 | <0.001 | 76% |
| Females | -0.530 | 0.060 | -0.648 | -0.412 | <0.001 | 80% |
| Left Side | -0.507 | 0.052 | -0.609 | -0.404 | <0.001 | 80% |
| Right Side | -0.624 | 0.062 | -0.747 | -0.501 | <0.001 | 76% |
| Overall | -0.558 | 0.040 | -0.637 | -0.479 | <0.001 | 78% |

3.3.11 Combined Results

These results were obtained by running the same analyses after calculating the mean for all different algorithm measurements of a single carrying angle. This method obtained an overall B value of -0.281 (95% CI: -0.349 to -0.213 $p < 0.001$) with an overall 80% validity. Further analysis based on variables revealed a higher validity result in the Age 20-40 group at 92%. Table 14 shows the detailed results obtained from each variable.

Table 14 Results for the Combined measurements showing B values, Standard Error, 95% Confidence Intervals, p values and validity all divided by the variables age, sex and side

| Group | B | Standard Error | 95% Confidence Interval | | p value | Validity |
|------------|--------|----------------|-------------------------|--------|---------|----------|
| | | | Lower | Upper | | |
| Age 1 | -0.371 | 0.088 | -0.546 | -0.195 | <0.001 | 73% |
| Age 5 | -0.361 | 0.070 | -0.500 | -0.221 | <0.001 | 76% |
| Age 9 | -0.318 | 0.079 | -0.475 | -0.161 | <0.001 | 75% |
| Age 11 | -0.152 | 0.066 | -0.284 | -0.020 | 0.024 | 83% |
| Age 20-40 | -0.207 | 0.075 | -0.357 | -0.058 | 0.007 | 92% |
| Males | -0.286 | 0.049 | -0.382 | -0.190 | <0.001 | 80% |
| Females | -0.274 | 0.049 | -0.371 | -0.177 | <0.001 | 80% |
| Left Side | -0.280 | 0.045 | -0.370 | -0.191 | <0.001 | 80% |
| Right Side | -0.283 | 0.054 | -0.388 | -0.177 | <0.001 | 79% |
| Overall | -0.281 | 0.035 | -0.349 | -0.213 | <0.001 | 80% |

4 Discussion

In the qualitative comparison, the Robinson operator was superior with the Kirsch operator closely behind. This revealed that the best methods for isolating bone edges in radiographic images of the extremities, especially in diaphyseal regions, are those which incorporate kernels in all eight compass directions. The Canny algorithm was also relatively more successful than other methods probably due to the incorporation of gradient angles, which is somewhat related to isolating edges in compass

directions. Interestingly however, these results did not coincide with the ones obtained from the carrying angle measurement comparisons. This indicates that, for the purposes of the automated algorithm used in this study, there are different factors which affect the measurement's validity.

When comparing the observer measurements, a strong positive inter-rater correlation was noted; however, the actual value for the ICC was significantly lower in this study, 0.643 (95% CI: 0.547 to 0.718) compared with the literature, 0.80 (95% CI: 0.75 – 0.84) [37]. This may have been due to the difference in the subject ages, number of elbows and the number of observers. In Goldfarb's study, the minimum age recruited was 12 and the total number of subjects was 178 with three different observers. The inclusion of the pediatric population at all stages of ossification as well as the increase in number to 500 with five different observers making measurements may have contributed to a lower ICC in our study.

Comparison of the algorithms revealed varying degrees of negative bias, the highest obtained in the LoG algorithm and the lowest in the Kirsch. Interestingly, after analysis of the variables, it was noted that the greatest number of significant bias came from the younger age groups and gradually decreased as the age increased. This indicated that skeletally immature bones inherently cause a bias in the automated readings of the carrying angle. This may be due to several reasons related to the radiographic characteristics of these bones such as: Poor contrast between the bone and the film, vague bone borders especially in non-ossified areas, rotated radiographic view related to questionable limb positioning due to the uncooperative nature of the patient and finally, short overall limb length which may affect the availability of adequate continuous bone edges.

In comparing the algorithm validity, the highest value for overall results came from the DoG algorithm (80%), while the highest value after variable analysis came from the age 20-40 group of the Frei-Chen algorithm (95%) followed closely by the same group in the DoG algorithm (94%) and the Hough Transform (93%). The lowest value for overall results was found in the LoG algorithm (55%), while the lowest value after variable analysis came from the age 1 group of the LoG algorithm (30%). As expected, algorithms with higher values for validity also had less bias than others.

With regards to the average processing time, the Robinson Operator (1min 13s) required the least time followed closely by the Frei-Chen (1min 16s) and Kirsch (1min 20s) Operator and then the DoG (1min 33s) and LoG (1min 37s) algorithms. Therefore, the best edge detection method based on all these factors was the DoG Algorithm which had a relatively low bias, high validity and low processing time. The Frei-Chen Algorithm was comparable but had a slightly lower validity while the Hough Transform had a much longer processing time. The worst edge detection method used in this study was found to be the LoG Algorithm due to its high bias and low validity.

The combined results showed the least bias, which was an expected consequence of averaging, but did not increase validity. They also suffered from the longest processing time due to the need to run all the edge detection methods before calculating the mean. This favored the usage of a single edge detector rather than a hybrid one.

The reasons which may have contributed to the DoG Algorithm being superior may be seen in the qualitative analysis which showed the highest edge thickness and internal noise with low edge accuracy and external noise. These factors can also be seen in the Frei-Chen Algorithm and the Hough Transform, which have obtained results comparable to the DoG Algorithm. Consequently, the most important

qualitative factors needed for automated angle measurements within diaphyseal areas of bone are: high edge thickness, high internal noise, low edge accuracy and low external noise. The LoG algorithm's poor results may have been due to its insensitivity towards external noise, which results in the incorrect approximation of the bone's edge.

5 Conclusion

The automated radiographic measurement of the carrying angle of the elbow is a very feasible and reliable process given the low bias and high validity of the algorithm when the DoG Algorithm is employed, especially if used strictly for mature bone. Since the lowest processing time was 1min 13s, the framework developed in this study may not be applicable for real-time processing or instant analysis results; however, it may be more practical to employ it as a batch processor. Nevertheless, if centralized on a high-end server, it could potentially provide fast results for clients, but this option has to be explored further.

ACKNOWLEDGEMENTS

This study was supported by the Medical Research Center at Hamad Medical Corporation. We thank Mr Yahya AlNouri for funding this project.

REFERENCES

- [1] Pope, T.L., et al., *Imaging of the Musculoskeletal System*. 2nd Edition ed. Expert Radiology Series 2008: Saunders. 2336.
- [2] Hak, D.J. and T.L. Gautsch, *A review of radiographic lines and angles used in orthopedics*. Am J Orthop (Belle Mead NJ), 1995. 24(8): p. 590-601.
- [3] Davies, E.R., *Chapter 5 - Edge Detection*, in *Computer and Machine Vision (Fourth Edition)*, E.R. Davies, Editor 2012, Academic Press: Boston. p. 111-148.
- [4] Grafova, L., et al., *Study of edge detection task in dental panoramic radiographs*. Dentomaxillofac Radiol, 2013. 42(7): p. 20120391.
- [5] Tariq, H. and S.M.A. Burney, *Contour Extraction of Femur and Tibia Condyles on Plain Anteroposterior (AP) Radiograph*. International Journal of Computer Applications, 2012. 52(15): p. 26-30.
- [6] Aydin, A., T. Ibrikci, and I.D. Akcali, *A hybrid image processing system for X-ray images of an external fixator*. Comput Methods Biomech Biomed Engin, 2012. 15(7): p. 753-9.
- [7] Zhang, J., et al., *Automatic Cobb measurement of scoliosis based on fuzzy Hough Transform with vertebral shape prior*. J Digit Imaging, 2009. 22(5): p. 463-72.
- [8] Conrozier, T., et al., *Reproducibility and sensitivity to change of a new method of computer measurement of joint space width in hip osteoarthritis. Performance of three radiographic views obtained at a 3-year interval*. Osteoarthritis Cartilage, 2009. 17(7): p. 864-70.

- [9] Qian, W., et al., *Tree-structured nonlinear filters in digital mammography*. IEEE Trans Med Imaging, 1994. 13(1): p. 25-36.
- [10] Leung, C.K., et al., *Novel approach for anterior chamber angle analysis: anterior chamber angle detection with edge measurement and identification algorithm (ACADEMIA)*. Arch Ophthalmol, 2006. 124(10): p. 1395-401.
- [11] Zhang, L.P., B.Y. Yang, and C.H. Wang, *[The analysis and comparison of different edge detection algorithms in ultrasound B-scan images]*. Zhongguo Yi Liao Qi Xie Za Zhi, 2006. 30(3): p. 170-2.
- [12] Lloret, R.L., et al., *Classification of left ventricular thrombi by their history of systemic embolization using pattern recognition of two-dimensional echocardiograms*. Am Heart J, 1985. 110(4): p. 761-5.
- [13] Pauwels, R., et al., *Automated implant segmentation in cone-beam CT using edge detection and particle counting*. Int J Comput Assist Radiol Surg, 2014. 9(4): p. 733-43.
- [14] Shi, J., et al., *Treatment response assessment of breast masses on dynamic contrast-enhanced magnetic resonance scans using fuzzy c-means clustering and level set segmentation*. Med Phys, 2009. 36(11): p. 5052-63.
- [15] Placidi, G., M. Alecci, and A. Sotgiu, *Post-processing noise removal algorithm for magnetic resonance imaging based on edge detection and wavelet analysis*. Phys Med Biol, 2003. 48(13): p. 1987-95.
- [16] Lin, X., et al., *Spinal cord atrophy and disability in multiple sclerosis over four years: application of a reproducible automated technique in monitoring disease progression in a cohort of the interferon beta-1a (Rebif) treatment trial*. J Neurol Neurosurg Psychiatry, 2003. 74(8): p. 1090-4.
- [17] Woodhead, H.J., et al., *Measurement of midfemoral shaft geometry: repeatability and accuracy using magnetic resonance imaging and dual-energy X-ray absorptiometry*. J Bone Miner Res, 2001. 16(12): p. 2251-9.
- [18] Garcia, E.V., et al., *Totally automatic definition of renal regions of interest from 99mTc-MAG3 renograms: validation in patients with normal kidneys and in patients with suspected renal obstruction*. Nucl Med Commun, 2010. 31(5): p. 366-74.
- [19] Drever, L.A., et al., *Comparison of three image segmentation techniques for target volume delineation in positron emission tomography*. J Appl Clin Med Phys, 2007. 8(2): p. 93-109.
- [20] Wang, Z., et al., *Semiautomatic segmentation and quantification of calcified plaques in intracoronary optical coherence tomography images*. J Biomed Opt, 2010. 15(6): p. 061711.
- [21] Rogowska, J. and M.E. Brezinski, *Image processing techniques for noise removal, enhancement and segmentation of cartilage OCT images*. Phys Med Biol, 2002. 47(4): p. 641-55.
- [22] Wang, Z., et al., *A combining method for tumors detection from near-infrared breast imaging*. Conf Proc IEEE Eng Med Biol Soc, 2005. 6: p. 6508-11.

- [23] Sivakamasundari, J., et al., *Fpga based hardware synthesis for automatic segmentation of retinal blood vessels in diabetic retinopathy images*. Biomed Sci Instrum, 2014. 50: p. 156-63.
- [24] Jia, X., H. Huang, and R. Wang, *A novel edge detection in medical images by fusing of multi-model from different spatial structure clues*. Biomed Mater Eng, 2014. 24(1): p. 1289-98.
- [25] Zhu, X., R.M. Rangayyan, and A.L. Ells, *Detection of the optic nerve head in fundus images of the retina using the Hough transform for circles*. J Digit Imaging, 2010. 23(3): p. 332-41.
- [26] Zhu, X. and R.M. Rangayyan, *Detection of the optic disc in images of the retina using the Hough transform*. Conf Proc IEEE Eng Med Biol Soc, 2008. 2008: p. 3546-9.
- [27] Chapman, N., et al., *Computer algorithms for the automated measurement of retinal arteriolar diameters*. Br J Ophthalmol, 2001. 85(1): p. 74-9.
- [28] Romary, D., J.F. Lerallut, and G. Fontenier, *Application of image processing techniques to gamma-angiography*. Comput Biomed Res, 1985. 18(5): p. 488-95.
- [29] Pijet, M., et al., *Fractal analysis of heart graft acute rejection microscopic images*. Transplant Proc, 2014. 46(8): p. 2864-6.
- [30] Irianto, J., D.A. Lee, and M.M. Knight, *Quantification of chromatin condensation level by image processing*. Med Eng Phys, 2014. 36(3): p. 412-7.
- [31] Ahammer, H. and T.T. DeVaney, *The influence of edge detection algorithms on the estimation of the fractal dimension of binary digital images*. Chaos, 2004. 14(1): p. 183-8.
- [32] Konstantinidis, I., A. Santamaria-Pang, and I. Kakadiaris, *Frames-Based Denoising in 3D Confocal Microscopy Imaging*. Conf Proc IEEE Eng Med Biol Soc, 2005. 1: p. 290-3.
- [33] Chang, M.H., et al., *Facial identification in very low-resolution images simulating prosthetic vision*. J Neural Eng, 2012. 9(4): p. 046012.
- [34] Daponte, J.S. and M.D. Fox, *Enhancement of chest radiographs with gradient operators*. IEEE Trans Med Imaging, 1988. 7(2): p. 109-17.
- [35] Potter, H.P., *The Obliquity of the Arm of the Female in Extension. The Relation of the Forearm with the Upper Arm in Flexion*. J Anat Physiol, 1895. 29(Pt 4): p. 488-91.
- [36] Chapleau, J., et al., *Validity of goniometric elbow measurements: comparative study with a radiographic method*. Clin Orthop Relat Res, 2011. 469(11): p. 3134-40.
- [37] Goldfarb, C.A., et al., *Elbow radiographic anatomy: measurement techniques and normative data*. J Shoulder Elbow Surg, 2012. 21(9): p. 1236-46.
- [38] Morrey, B.F., *Morrey's The Elbow and Its Disorders*. 4th Edition ed2009: Saunders. 1232.
- [39] Sobel, I. and G. Feldman, *A 3x3 Isotropic Gradient Operator for Image Processing*, 1968.

- [40] Scharr, H., *Optimale Operatoren in der digitalen Bildverarbeitung*, 2000, Universitätsbibliothek.
- [41] Prewitt, J.M.S., *Object Enhancement and Extraction*, in *Picture processing and Psychopictorics*, B.S. Lipkin and A. Rosenfeld, Editors. 1970, Academic Press: New York.
- [42] Frei, W. and C. Chung-Ching, *Fast Boundary Detection: A Generalization and a New Algorithm*. *Computers, IEEE Transactions on*, 1977. C-26(10): p. 988-998.
- [43] Kirsch, R.A., *Computer determination of the constituent structure of biological images*. *Comput Biomed Res*, 1971. 4(3): p. 315-28.
- [44] Robinson, G.S., *Edge detection by compass gradient masks*. *Computer Graphics and Image Processing*, 1977. 6(5): p. 492-501.
- [45] Klette, R., *Concise Computer Vision: An Introduction into Theory and Algorithms*. Undergraduate Topics in Computer Science 2014: Springer.
- [46] Marr, D. and E. Hildreth, *Theory of Edge Detection*. *Proceedings of the Royal Society of London B: Biological Sciences*, 1980. 207(1167): p. 187-217.
- [47] Canny, J., *A Computational Approach to Edge Detection*. *Pattern Analysis and Machine Intelligence, IEEE Transactions on*, 1986. PAMI-8(6): p. 679-698.
- [48] Duda, R.O. and P.E. Hart, *Use of the Hough transformation to detect lines and curves in pictures*. *Commun. ACM*, 1972. 15(1): p. 11-15.
- [49] Paraskevas, G., et al., *Study of the carrying angle of the human elbow joint in full extension: a morphometric analysis*. *Surg Radiol Anat*, 2004. 26(1): p. 19-23.
- [50] Koch, G.G., *Intraclass correlation coefficient*, in *Encyclopedia of Statistical Sciences*, S. Kotz and N.L. Johnson, Editors. 1982, John Wiley & Sons: New York. p. 213-217.